Dynamics of Three-Tori in a Periodically Forced Navier-Stokes Flow

J. M. Lopez

Department of Mathematics, Arizona State University, Tempe, Arizona 85287-1804

F. Marques

Departament de Física Aplicada, Universitat Politècnica de Catalunya, Mòdul B5 Campus Nord, 08034 Barcelona, Spain
(Received 1 March 2000)

Three-tori solutions of the Navier-Stokes equations and their dynamics are elucidated by use of a global Poincaré map. The flow is contained in a finite annular gap between two concentric cylinders, driven by the steady rotation and axial harmonic oscillations of the inner cylinder. The three-tori solutions undergo global bifurcations, including a new gluing bifurcation, associated with homoclinic and heteroclinic connections to unstable solutions (two-tori). These unstable two-tori act as organizing centers for the three-tori dynamics. A discrete space-time symmetry influences the dynamics.

Most natural systems contain more than two frequencies and the behavior of systems with three frequencies is still not well understood; it is not even known whether there are universal three-frequency behaviors [1]. Newhouse *et al.*'s theorem [2] raised the question as to whether three-tori solutions would be observable in physical systems. Subsequent analysis [3] suggests that three-tori solutions could be expected in typical nonlinear dynamical systems. Experimental evidence of three-tori have been reported in laser experiments, Rayleigh-Bénard convection, semiconductors, and electric circuits [4]. Also, examples of three-tori from low-dimensional systems of equations have been reported [5]. To date, known examples of three-tori in Navier-Stokes type systems have been reported for studies where the equations have been discretized spectrally and only a small number of modes were retained [6]. While the truncated systems were derived from the Navier-Stokes equations, their solutions are not solutions of Navier-Stokes as the nonlinear terms transfer energy to modes not included in the truncated systems.

The results presented here are of three-tori solutions from a fully resolved numerical computation of the Navier-Stokes equations with no-slip boundary conditions, restricted to an axisymmetric subspace, and as such, the obtained three-tori solutions are solutions to the full Navier-Stokes equations. The system in question is the flow between two coaxial cylinders of finite extent with stationary top and bottom end walls. The outer cylinder is also stationary, while the inner cylinder rotates at constant angular velocity Ω_i and oscillates in the axial direction with velocity $W \sin \Omega_f t$. Its radius is r_i, the radius of the outer stationary cylinder is r_o, and their length is L; the annular gap between the cylinders is $d = r_o - r_i$. These parameters are combined to give the following nondimensional governing parameters: the radius ratio $e = r_i/r_o$, the length to gap ratio $\Lambda = L/d$, the Couette flow Reynolds number $\text{Ri} = d r_i \Omega_i / \nu$, the axial Reynolds number $\text{Ra} = dW/\nu$, and the nondimensional forcing frequency $\omega_f = d^2 \Omega_f / \nu$, where ν is the kinematic

viscosity of the fluid. The basic flow is time periodic with period $T_f = 2\pi/\omega_f$ and synchronous with the forcing, and it is independent of the azimuthal coordinate.

The incompressible Navier-Stokes equations governing this problem are invariant to two symmetry groups. One corresponds to rotations around the common axis of the cylinders, SO(2). The other, Z_2, is generated by the discrete symmetry S, involving time and the axial coordinate; it is a reflection about the midplane orthogonal to the axis with a simultaneous time translation of a half-forcing period, satisfying $S^2 = I$. The complete symmetry group of this problem is SO(2) $\times$ Z_2 [7]. In this study we solve the system in an axisymmetric subspace invariant to SO(2). Linear stability analyses in the limit $\Lambda \to \infty$ have shown that over an extensive range of parameter space, the primary bifurcation is to an axisymmetric state, periodic in the axial direction and synchronous with the forcing, and only in small windows of parameter space have nonaxisymmetric flows been observed [8]. Therefore the only nontrivial symmetry of the axisymmetric system considered is S. This symmetry has many consequences for the dynamics and bifurcations that the system can experience; in particular, it inhibits period doubling bifurcations [9].

Compelling theoretical and experimental evidence on the importance of end wall effects in the unforced Taylor-Couette flow is provided by [10], even for very large aspect ratio systems. Instead of having a continuum of possible axial wave numbers as in the $\Lambda \to \infty$ case, with Λ finite there is only a discrete spectrum, and the transition to flows with axial variations originates in the end wall layers and exists for all finite Reynolds numbers Ri. A preliminary numerical study of the flow with end walls was made in [7]. The boundary conditions where the end walls meet the moving inner cylinder are discontinuous, and an accurate numerical treatment that mimics the experimental conditions has been used to deal with this discontinuity [11]. The nonlinear effects induced by the finite aspect ratio and the presence of end walls were investigated with an efficient and accurate spectral-projection method for solving

the fully nonlinear axisymmetric Navier-Stokes equations [7,11]. Two scenarios were considered: varying, respectively, the forcing amplitude Ra and the Couette flow Reynolds number Ri while keeping other parameters fixed. In the former case, with Ri = 200, the nonlinear response of the system was synchronous with the forcing frequency, and as Ra was reduced the flow underwent a smooth transition from a state whose axial variations are confined to the end wall regions to a state with Taylor cells throughout the entire annulus. As Ra was further reduced, additional solution branches, all synchronous with the forcing, were encountered. When Ra was fixed and Ri increased, a Naimark-Sacker bifurcation [12] led to flow on a two-torus. Such a bifurcation is peculiar to the finite aspect ratio situation, with the unsteady coupling between the end wall vortices and the jets emanating from the boundary layer on the inner cylinder.

In this Letter, the axisymmetric Navier-Stokes equations have been solved with the spectral scheme described in [7], using 80 axial and 64 radial modes, and a time step $\delta t = T_f/200$. We only consider variations in Ri, keeping all other parameters fixed ($\Lambda = 10$, $e = 0.905$, Ra = 80, $\omega_f = 30$). We have located a range (Ri $\in$ [280.89, 281.26]) where stable three-tori solutions exist. The identification of such solutions has been significantly helped due to the imposed periodic forcing, which implies the existence of a global Poincaré map, P, for the system (i.e., strobing at the forcing frequency ω_f). The power spectral density (PSD) of the time series of Γ, the vertical angular momentum at a convenient Gauss-Lobato point in the annulus, $Q(r = r_i + 0.573, z = 0.969)$, has a main peak at the forcing frequency, $\omega_f = 30$, a second frequency at $\omega_s \approx 5.2$, and their linear combinations since these are incommensurate. The frequency ω_s has been found to be associated with the coupling between the end wall vortices and the sidewall jets [7]. The PSD also possesses a very low frequency ω_{VLF} which is 3 orders of magnitude smaller than ω_s. Because of the large spectral gaps between these three incommensurate frequencies we have been able to unambiguously characterize these solutions as three-tori.

Over the range of Ri where three-tori solutions exist, $\omega_s = 5.2 \pm 3\%$. In contrast, $T_{VLF} = 2\pi/\omega_{VLF}$ experiences dramatic changes over this range, as shown in Fig. 1. This figure indicates that there are two Ri values where T_{VLF} becomes unbounded. For ease of discussion, we now represent three-tori as limit cycles and two-tori as fixed points. This analogy works since the two suppressed frequencies, ω_f and ω_s, are almost constant (in fact, ω_f is constant), over the range of Ri of interest, and they do not play an essential role in the dynamics near the bifurcation points. Infinite-period bifurcations are usually associated with homoclinic or heteroclinic behavior. The two most typical are the following: (i) A limit cycle collides with a hyperbolic fixed point resulting in a homoclinic connection and then vanishes, and (ii) a saddle node occurs on
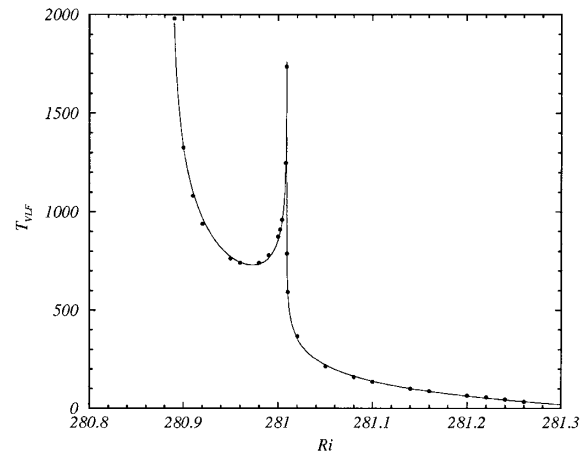

FIG. 1. Variation of $T_{VLF} = 2\pi/\omega_{VLF}$ with Ri. Symbols are computed values, and solid lines are log fits.

the limit cycle. These two scenarios are distinguished by the asymptotic behavior of the period of the limit cycle as the bifurcation point is approached. In case (i) the period close to the bifurcation point would have the form $T_{VLF} \sim c \ln(1/|Ri - Ri_{crit}|) + d$ [13], while in case (ii) $T_{VLF} \sim c/\sqrt{|Ri - Ri_{crit}|} + d$ [12]. Our computed T_{VLF} fits the logarithmic form very well, whereas it does not adjust to the square root form. The fitted logarithmic curves are the solid lines in Fig. 1, and the symbols are the computed periods. The fits are uniformly good over the whole range of existence of the three-tori, strongly suggesting that the homoclinic/heteroclinic behavior dominates the dynamics over the whole interval. The expression for the logarithmic profile in the first section is given by

$$T_{VLF} = \lambda_{het}^{-1} \ln \frac{1}{|Ri - Ri_{het}|}$$
$$+ \lambda_{hom}^{-1} \ln \frac{1}{|Ri - Ri_{hom}|} + c.$$

The logarithmic fits give the critical Ri for the two infinite-period bifurcations, $Ri_{het} = 280.887\,36$ and $Ri_{hom} = 281.008\,84$. The factors λ are the eigenvalues corresponding to the unstable direction of the hyperbolic fixed points (in our case, these are unstable two-tori) [13]. The values obtained are $\lambda_{het} = 2.43 \times 10^{-3}$ and $\lambda_{hom} = 5.81 \times 10^{-3}$.

Figure 2(a) shows the projection of the Poincaré map P into the plane (U, Γ) (radial velocity and vertical angular momentum at the Gauss-Lobato point Q) at Ri = 280.89, the closest Ri value to Ri_{het} computed. This clearly indicates that the solution trajectory spends a long time close to not one, but two unstable two-tori, appearing as cycles in the Poincaré map P. This is due to the S symmetry of the system. The three-torus is S invariant, whereas the unstable two-tori to which it connects heteroclinically at Ri_{het} are not S symmetric, but are related to each other via the S symmetry. The three-torus collides with the two unstable two-tori simultaneously due to the S symmetry.
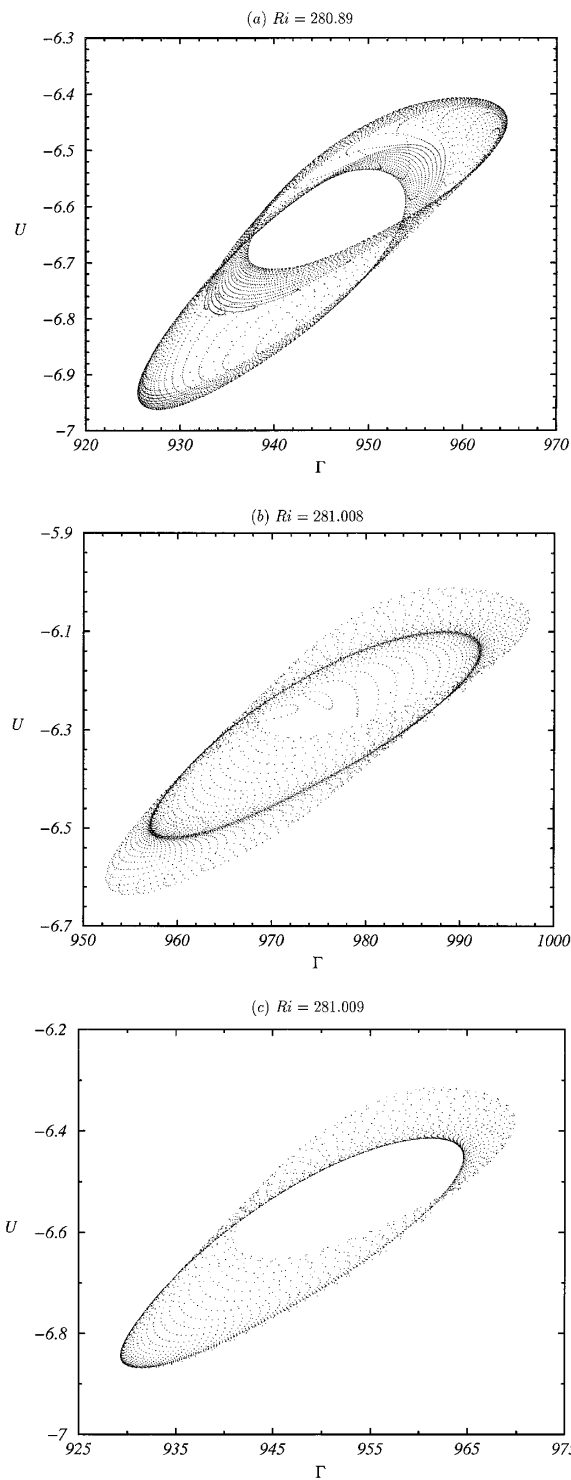
973

FIG. 2. Projection of the iterates of the Poincaré map onto the $(U, \Gamma)_Q$ plane for Ri as indicated.

The infinite-period bifurcation at Ri = Ri$_{hom}$ is more complicated as three-tori exist on both sides of the bifurcation. Approaching Ri$_{hom}$ from below, the three-torus is S symmetric and approaches an unstable two-torus which is also S symmetric. This is seen in the projection of the Poincaré map for Ri = 281.008, which is very close to

Ri$_{hom}$. Figure 2(b) shows the presence of two distinct fast homoclinic excursions. At the bifurcation point, Ri$_{hom}$, there exist two homoclinic loops that are related by the S symmetry. This is illustrated schematically in Fig. 3.

For Ri > Ri$_{hom}$, but close to the bifurcation, the behavior is qualitatively different. Figure 2(c) shows at Ri = 281.009 the existence of a three-torus close to an unstable two-torus with a single homoclinic excursion. We also note from Fig. 1 that for Ri > Ri$_{hom}$, the period T_{VLF} is significantly reduced from that when Ri < Ri$_{hom}$. Beyond Ri$_{hom}$, the double homoclinic loop splits into two three-tori as shown in the schematic Fig. 3. The solution in Fig. 2(c) corresponds to one of these three-tori, which is no longer S symmetric. We have explicitly computed the S-related partners for Ri > Ri$_{hom}$ by applying the symmetry S to a trajectory on the first obtained three-torus; a trajectory on a different three-torus results. These two distinct three-tori are S-symmetrically related. We have not been able to continue the three-tori solution branches beyond Ri = 281.26; the system evolves to another one corresponding to a two-torus branch that has previously been described [7].

The range of Ri where three-tori exist consists of two branches; for Ri$_{het}$ < Ri < Ri$_{hom}$ there is a single S symmetric three-torus and for Ri > Ri$_{hom}$ a pair of nonsymmetric, but symmetrically related, three-tori. The first branch starts in a heteroclinic bifurcation schematically
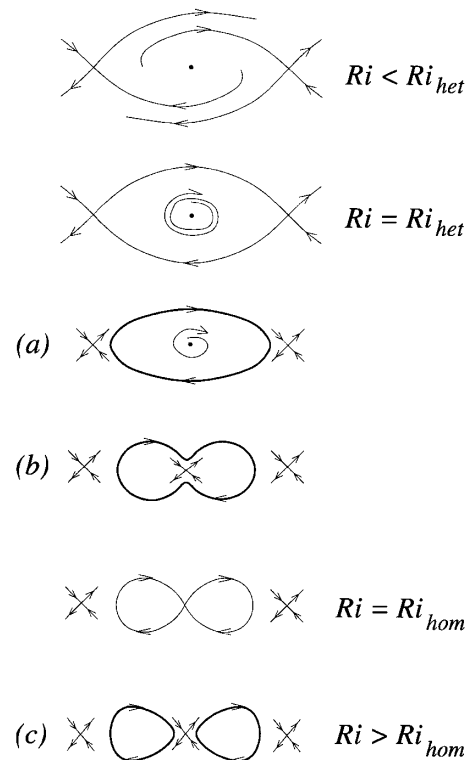

FIG. 3. Schematic of the bifurcation sequence for the three-tori solutions. In this schematic, two-tori are represented as fixed points and three-tori as cycles. The labels (a), (b), and (c) correspond to the three parts of Fig. 2.

shown in Fig. 3, and is related to the second branch via a homoclinic bifurcation at $Ri = Ri_{hom}$. In this homoclinic bifurcation an S-symmetric three-torus splits in two S-related three-tori. Analogous gluing bifurcations of limit cycles in systems with Z_2 symmetry have been analyzed in [14], and in [15] for systems with more complex (D_4) symmetries. We have found for the first time a gluing bifurcation of three-tori in a real fluid system.

As noted in [7], the two-tori correspond physically to the interaction of jets emanating from the sidewall with the end wall layers. This interaction leads to the ω_s frequency. The schematic saddles in Fig. 3 are unstable two-tori solutions of this type. These unstable states play a key role in the dynamics, acting as organizing centers [16]. The three-tori solutions reported here correspond to slow drifts between these distinct unstable two-tori states. Similar very low frequency states have also been observed experimentally [17] in an unforced Taylor-Couette flow with aspect ratio of order 10, as is the aspect ratio in our computations. Since their system was unforced, the VLF states manifested themselves as two-tori. Two-torus VLF states following the breaking of a Z_2 symmetry have also been obtained numerically in a rotating cylindrical system where a sidewall jet interacts with Ekman layers on the end walls [18].

In summary, we have observed and analyzed interesting nonchaotic dynamics of three-tori in a real fluid system, obtained by numerically solving the Navier-Stokes equations in an axisymmetric subspace. The organizing centers of the dynamics are unstable two-tori states that correspond to different modes of interaction between the end wall layers and the outgoing wall jets. The example shown in this Letter exhibits a gluing bifurcation of three-tori and points to some general considerations: (i) unstable two-tori play a key role as organizing centers of the dynamics, (ii) the bifurcation diagrams are strongly affected by the presence of symmetries, and (iii) close analogies exist between the three-tori bifurcations we have found and well-known bifurcations of fixed points and limit cycles that have been found both numerically and experimentally [15,17].

[1] J. A. Glazier and A. Libchaber, IEEE Trans. Circuits Syst. **35**, 790 (1988).

[2] S. Newhouse, D. Ruelle, and F. Takens, Commun. Math. Phys. **64**, 35 (1978).

[3] J. H. Curry and J. A. Yorke, Springer Notes Math. **668**, 48 (1978); C. Grebogi, E. Ott, and J. A. Yorke, Phys. Rev. Lett. **51**, 339 (1983); Physica (Amsterdam) **15D**, 354 (1985).

[4] R. W. Walden, P. Kolodner, A. Passner, and C. M. Surko, Phys. Rev. Lett. **53**, 242 (1984); D. J. Biswas and R. G. Harrison, Phys. Rev. A **32**, 3835 (1985); P. S. Linsay and A. W. Cumming, Physica (Amsterdam) **40D**, 196 (1989); T. Schneider, H. Heng, and W. Martienssen, Europhys. Lett. **22**, 499 (1993).

[5] P. M. Battelino, Phys. Rev. A **38**, 1495 (1988); P. M. Battelino, C. Grebogi, E. Ott, and J. A. York, Physica (Amsterdam) **39D**, 299 (1989).

[6] V. Franceschini, Physica (Amsterdam) **6D**, 285 (1983); C. Giberti and R. Zanasi, Physica (Amsterdam) **65D**, 300 (1993).

[7] J. M. Lopez, F. Marques, and J. Shen, Fluid Dyn. Res. **27**, 91 (2000).

[8] F. Marques and J. M. Lopez, J. Fluid Mech. **348**, 153 (1997); Physica (Amsterdam) **136D**, 340 (2000); A. Y. Weisberg, I. G. Kevrekidis, and A. J. Smits, J. Fluid Mech. **348**, 141 (1997).

[9] J. W. Swift and K. Wiesenfeld, Phys. Rev. Lett. **52**, 705 (1984).

[10] T. B. Benjamin and T. Mullin, Proc. R. Soc. London A **377**, 221 (1981).

[11] J. M. Lopez and J. Shen, J. Comput. Phys. **139**, 308 (1998).

[12] Y. A. Kuznetsov, *Elements of Applied Bifurcation Theory* (Springer-Verlag, Berlin, 1998), 2nd ed.

[13] P. Gaspard, J. Phys. Chem. **94**, 1 (1990).

[14] P. Glendinning, Phys. Lett. **103A**, 163 (1984).

[15] D. Ambruster, B. Nicolaenko, N. Smaoui, and P. Chossat, Physica (Amsterdam) **95D**, 81 (1996).

[16] T. Mullin, *The Nature of Chaos* (Oxford University Press, Oxford, 1993).

[17] J. von Stamm, U. Gerdts, T. Buzug, and G. Pfister, Phys. Rev. E **54**, 4938 (1996); F. H. Busse, G. Pfister, and D. Schwabe, Springer Lect. Notes Phys. **m55**, 86 (1998).

[18] J. M. Lopez, Phys. Fluids **7**, 2700 (1995).